Total words: 7209

Photoelectro-Fenton as post-treatment for electrocoagulated benzophenone-3-loaded synthetic and urban wastewater

Zhihong Ye, Juliana R. Steter, Francesc Centellas, Pere Lluís Cabot, Enric Brillas*, Ignasi Sirés*

Laboratori d'Electroquímica dels Materials i del Medi Ambient, Departament de Química Física, Facultat de Química, Universitat de Barcelona, Martí i Franquès 1-11, 08028 Barcelona, Spain

* Corresponding author: *E-mail address*: brillas@ub.edu (E. Brillas)

E-mail address: i.sires@ub.edu (I. Sirés)

Abstract

The removal of benzophenone-3 (BP-3), a ubiquitous pollutant in municipal wastewater treatment facilities, was optimal by means of a sequential electrocoagulation (EC) / UVA photoelectro-Fenton (PEF) treatment. Overall mineralization was attained upon combination of EC (Fe/Fe cell, 15 mA cm^{-2}, 20 min) with PEF (boron-doped diamond/air-diffusion cell, 33.3 mA cm^{-2}, 720 min), being superior to EC/electro-Fenton (EF) and requiring shorter time than single PEF. In EC, an Al/Al cell yielded the largest removal of BP-3 in a simulated matrix at pH 11.0 due to precipitation of its neutral form caused by a substantial pH drop, with optimum current density of 15 mA cm^{-2}. EC of BP-3-loaded urban wastewater at natural pH was quite effective also with a Fe/Fe cell, being preferred since it provided the required metal catalyst for subsequent treatment. Among the electrochemical advanced oxidation processes tested, PEF was superior to electrochemical oxidation with electrogenerated H_2O_2 (EO-H_2O_2) and EF, especially when using the boron-doped diamond instead of a RuO_2-based anode, due to the oxidation of generated active chlorine and hydroxyl radicals, along with the photolytic action of UVA irradiation. GC-MS revealed the formation of 14 cyclic products in PEF treatment, two of them being also formed during EC.

Keywords: Benzophenone-3; Electrocoagulation; Electro-Fenton; Oxidation products; Photoelectro-Fenton; Wastewater treatment

1. Introduction

Benzophenone-3 (BP-3, $C_{14}H_{10}O_3$, 2-hydroxy-4-methoxybenzophenone, M = 228.25 g mol^{-1}), also called oxybenzone, is widely employed as sunscreen agent due to its large ability to absorb UV light, limited photodecomposition and high lipophilicity (Abdallah et al., 2015). It is an active ingredient in lotions and personal care products including bath oils, soaps, mascaras and anti-aging creams (Downs et al., 2016). A release of 14,000 ton y^{-1} of BP-3 into the aquatic environment is estimated via wash-off from skin and clothes or indirectly via solid waste landfill leachate and wastewater treatment facilities (WWTFs), thereby being detected in natural water bodies, soil, fish and even in human milk (Gago-Ferrero et al., 2013; Downs et al., 2016). It has reached up to 7800 ng L^{-1} in untreated municipal wastewater, being reduced to 700 ng L^{-1} upon treatment (Liu et al., 2012). It has also been detected within the 10-20 ng g^{-1} range in sewage sludge and 3-21 ng g^{-1} in fish (Liu et al., 2012). Its potential toxicity arises from endocrine disruption, genotoxicant actuation, pro-carcinogenic activity, mutagenic ability of derivatives and skin penetration in humans (Downs et al., 2016).

The water solubility of BP-3 (pK_a = 9.65 (Gilberta et al., 2016; Li et al., 2016) is very high at pH > 10 where its anionic form predominates, whereas its neutral form prevailing at pH ≤ 9 has very low solubility (< 5 mg L^{-1}). Effective removal of BP-3 from synthetic aqueous matrices at pH 3-9 has been attained by biodegradation (Liu et al., 2012), ultrasound (Zúñiga-Benítez et al., 2016c), ozonation and peroxone oxidation (Gago-Ferrero et al., 2013), membrane catalytic ozonation (Guo et al., 2016), photo-Fenton (Zúñiga-Benítez et al., 2016b), TiO_2/photocatalysis (Zúñiga-Benítez et al., 2016a) and UV/H_2O_2 (Gong et al., 2015). Most of these works only determined the decay kinetics of BP-3 at concentrations ≤ 1 mg L^{-1}, but did not assess the formation of hydroxylated and/or chlorinated derivatives, potentially more toxic than BP-3 (Li et al., 2016).

Recently, electrochemical advanced oxidation processes (EAOPs) have received great attention for wastewater remediation because they cause large mineralization of aqueous solutions containing organic pollutants (Asghar et al., 2015; El-Ashtoukhy et al., 2017; Silva et al., 2018). The most typical EAOP is electrochemical oxidation (EO), which can be utilized with electrogenerated H_2O_2 (EO-H_2O_2) (Panizza and Cerisola, 2009; Sirés et al., 2014; Särkkä et al., 2015). Fenton-based EAOPs such as electro-Fenton (EF) (Brillas et al., 2009; Martínez-Huitle et al., 2015; Moreira et al., 2017) and photoelectro-Fenton (PEF) (Brillas et al., 2009; Brillas, 2014) are even more powerful. Their good performance results from the generation of the powerful oxidant hydroxyl radical ($^{\bullet}OH$). UVA light employed to irradiate the solution in PEF photolyzes photoactive intermediates, accelerating their conversion into CO_2 and making it the most efficient EAOP (Wang et al., 2008; Salazar et al., 2012; Urzúa et al., 2013). However, main drawbacks for PEF application include long time needed to destroy large contents of organic matter and poor light penetration when solutions contain colloidal particles. To overcome these limitations, the use of electrocoagulation (EC) as pre-treatment has been recently envisaged (Thiam et al., 2014; Bocos et al., 2016). EC involves the in situ generation of coagulants from dissolution of an appropriate sacrificial anode (Fe or Al), forming flocs that precipitate and adsorb colloids and organics. Partial oxidation of the organic matter with generated $^{\bullet}OH$ and active chlorine (Cl_2/HClO/ClO^-) in the presence of Cl^- seems also feasible (Ghernaout et al., 2011; Ghernaout, 2013; Demirbas and Kobya, 2017). To date, sequential EC/EAOPs have only by examined by the dye Tartrazine (Thiam et al., 2014) and the antiseptic bronopol (Bocos et al., 2016) in synthetic solutions with ultrapure water. However, the viability of EC/EAOPs coupling has not been tested yet for urban wastewater, which contains natural organic water (NOM) that may exert some influence on the degradation of organic pollutants. Under these conditions, the treatment at natural pH can be performed, relying on the good performance of heterogeneous Fenton-like systems (Cheng et al., 2016, 2018a, 2018b).

The present article reports the first EC/EAOPs coupling for the removal of an organic pollutant spiked into an effluent from primary wastewater treatment. BP-3 was selected as model molecule, being determined its decay kinetics and total organic carbon (TOC) removal. First, the EC treatment of BP-3 in a simulated matrix with the same ionic composition as the urban wastewater, at pH 11.0, was tested with cells containing Al or Fe anode to elucidate the role of the BP-3 acid-base equilibrium. Analogous EC trials were made using the real effluent at natural pH, where the neutral form was predominant. Then, the single EO-H_2O_2, EF and PEF treatments of urban wastewater at natural pH spiked with BP-3 were studied using a RuO_2-based or boron-doped diamond (BDD) anode and an air-diffusion cathode. Intermediates of BP-3 formed by EC and PEF were identified by gas chromatography-mass spectrometry (GC-MS), leading to a route for BP-3 removal. Finally, sequential EC/EF and EC/PEF of BP-3-loaded urban wastewater were examined to compare their performance with that of single EAOPs.

2. Experimental

2.1. Chemicals

BP-3 (98% purity) was provided by Sigma-Aldrich. The salts used as supporting electrolytes were purchased from Panreac and Merck. Analytical grade $FeSO_4 \cdot 7H_2O$ used as catalyst was purchased from J.T. Baker. High-quality Millipore Milli-Q water (> 18 MΩ cm) was used to prepare all synthetic solutions. Other chemicals were of HPLC or analytical grade from Panreac and Merck.

2.2. Urban wastewater

The real sample was collected from the primary clarifier of a WWTF located near Barcelona. This facility treated 50,000 $m^3\ d^{-1}$ of mixed urban and industrial wastewater. After

collection, the urban wastewater was preserved in a refrigerator at 4 ºC and was used in the next 15 d to prevent anaerobic degradation.

According to Table S1, the primary treated effluent had pH ~ 8.0 and low conductivity, total carbon (TC), TOC and TN. Na^+ prevailed over cations like K^+, Ca^{2+} and Mg^{2+}, with insignificant total iron content. Among anions, Cl^- predominated over SO_4^{2-}, both at relatively high contents. Table S2 summarizes the characteristics of 18 organic compounds detected for the raw wastewater by GC-MS, which included 17 cyclic (3 of them aromatic and 5 with N as heteroatom) and 1 aliphatic compounds. Worth mentioning, our target pollutant BP-3 was also contained in the real effluent.

2.3. Electrolytic systems

The electrolytic trials were made in an undivided, open glass cell with a double jacket for circulation of thermostated water at 35 °C, under vigorous stirring by a magnetic follower. This temperature was selected because it is the maximum value to operate without significant water evaporation from the solution, thus obtaining the best reactivities during the degradation trials with reproducible measurements. In EC, the anode was an iron or aluminum plate with immersed area of 10 cm^2. The same materials as well as stainless steel (AISI 304 or AISI 316L) plates of the same area were tested as cathode. The electrode pairs were placed alternately in parallel at distance of 1.0 cm. In EAOPs, the anode was a RuO_2-based plate from NMT Electrodes (Pinetown, South Africa) or a BDD thin-film on Si supplied by NeoCoat (La Chaux-de-Fonds, Switzerland). The cathode was a carbon-PTFE air-diffusion electrode from E-TEK (Division of De Nora N.A., Inc.), mounted as described elsewhere (Steter et al., 2016) and fed with air pumped at 1 L min^{-1} for continuous H_2O_2 generation. The area of all electrodes was 3 cm^2 and their distance was 1.0 cm, being prepared as described elsewhere prior to first use (Thiam et al., 2014). PEF was made under UVA irradiation (λ_{max} = 360 nm, 5 W m^{-2}) provided by a Philips fluorescent black light blue tube.

Fresh solutions of pollutant contained 30 mg C L^{-1} BP-3 (0.178 mM) in simulated matrix (pH 11.0, stirring for 2 h) or 4 mg C L^{-1} BP-3 (0.024 mM) in urban wastewater (natural pH, stirring for 12 h). In the sequential EC/EAOPs, the EC-treated solutions were centrifuged for 10 min at 4100 rpm to remove the sludge and easily collect the supernatant for post-treatment.

2.4. Analytical procedures

The electrical conductance and pH were measured on a Metrohm 644 conductometer and a Crison GLP 22 pH-meter. Trials were carried out at constant current density (*j*) using an Amel 2053 potentiostat-galvanostat. H_2O_2 concentration was determined using a Shimadzu 1800 UV/vis spectrophotometer at 25 °C following a standard methodology (Welcher, 1975). Samples withdrawn from treated solutions were microfiltered (0.45 μm) before analysis. TOC was determined on a Shimadzu TOC-VCNS analyzer. Total nitrogen and concentration of anions and cations, including total iron, were obtained as reported elsewhere (Ridruejo et al., 2017).

BP-3 content at λ = 277 nm and short-linear aliphatic carboxylic acids at λ = 210 nm were determined by reversed-phase and ion-exclusion HPLC using a Waters LC, as previously reported (Salazar et al., 2012; Ridruejo et al., 2017). In the former case, an acetonitrile/10 mM KH_2PO_4 (50:50 v/v) mixture at 1 mL min^{-1} was used as mobile phase and BP-3 was detected at retention time (t_r) = 19.2 min, with limit of quantification = 0.15 mg L^{-1} and limit of detection = 0.05-0.10 mg L^{-1}.

Table S3 summarizes all the electrochemical characteristics of the single and sequential assays performed with simulated matrix, Na_2SO_4 and urban wastewater. All experiments were made in duplicate and average results are given, with the corresponding error bars in figures.

The organic components of the raw urban wastewater and electrolyzed solutions under EC and PEF conditions were extracted with CH_2Cl_2 (3 × 25 mL). The resulting organic solution was dried over anhydrous Na_2SO_4, filtered and concentrated to ca. 1 mL to be analyzed by GC-

MS using optimized analytical conditions (Salazar et al., 2012) and a NIST05 MS library for interpretation. The analysis was made with an Agilent Technologies system composed of a 6890N gas chromatograph with a 7683B series injector and a 5975 mass spectrometer in electron impact mode at 70 eV. A nonpolar Agilent J&W DB-5 or a polar HP INNOWax column of 0.25 μm, 30 m × 0.25 mm, was employed. The temperature ramp was: 36 ºC for 1 min, 5 ºC min^{-1} up to 300 ºC and hold time 10 min. The inlet, source and transfer line operated at 250, 230 and 280 ºC.

3**. Results and discussion**

3.1. EC treatment of BP-3 in a simulated matrix at pH 11.0

Comparative EC trials were made with 150 mL of 30 mg C L^{-1} BP-3 in simulated matrix at pH 11.0 using an Al or Fe anode. The composition of the simulated matrix mimicked the main ion content of urban wastewater (Table S1), with 1.8 mS cm^{-1} conductivity. Cathodes of the same materials as well as of AISI 304 or AISI 316L were employed to test the performance of each anode/cathode cell for 60 min at 10 mA cm^{-2}, without pH regulation. Fig. 1a and b shows a gradual decay of normalized TOC with time in all cases, but profiles depended on each material. For each anode, the best anode/cathode combinations were Al/Al and Fe/Fe, attaining 47.0% and 17.7% TOC removals with final pH of 9.5 and 10.8 and conductivities of 2.2-2.6 mS cm^{-1}. Moreover, BP-3 concentration decays reached 67.2% and 28.9% for these two cells.

Al^{3+} and Fe^{2+} are released to the bulk from sacrificial Al and Fe anodes via reactions (1) and (2) (Thiam et al., 2014; Bocos et al., 2016; Steter et al., 2016). At the cathode, H_2 gas and OH^- are produced from reaction (3), favoring the formation of insoluble metal hydroxides from reactions (4)-(6) (Ghernaout, 2013; Khandegar and Saroha, 2013; Brillas and Martínez-Huitle, 2015).

$$Al_{(s)} \rightarrow Al^{3+}_{(aq)} + 3e^- \quad (1)$$

$$Fe_{(s)} \rightarrow Fe^{2+}_{(aq)} + 2e^- \quad (2)$$

$$2H_2O + 2e^- \rightarrow H_{2(g)} + 2OH^- \quad (3)$$

$$Al^{3+}_{(aq)} + 3OH^- \rightarrow Al(OH)_{3(s)} \quad (4)$$

$$Fe^{2+}_{(aq)} + 2OH^- \rightarrow Fe(OH)_{2(s)} \quad (5)$$

$$4Fe^{2+}_{(aq)} + 10H_2O + O_{2(g)} \rightarrow 4Fe(OH)_{3(s)} + 8H^+_{(aq)} \quad (6)$$

The insoluble $Al(OH)_3$ and $Fe(OH)_n$ flocs with large surface area precipitate removing pollutants by surface complexation, electrostatic attraction or sweep coagulation in Al/Al and Fe/Fe cells (Ghernaout, 2013; Khandegar and Saroha, 2013). It is noticeable that higher BP-3 and TOC abatements were obtained using AISI 304/AISI 316L and AISI 316L/AISI 316L cells as compared to Fe/Fe cell (data not shown), due to the enhanced coagulation ability by the production of hydroxides from other metallic species contained in sacrificial stainless steel anodes, e.g., Cr-, Ni-, Mn- and Mo-based. However, the potential toxicity of these hydroxides prevent the large use of such anodes in EC. Fig. 1a and b also evidences the influence of the cathode material on TOC decay, suggesting the co-existence of reductive routes where BP-3 and its byproducts can be transformed at the cathode surface into compounds with different tendency to be coagulated.

The greater BP-3 and TOC abatements using the Al/Al cell could be plausibly ascribed to the substrate precipitation from the pH decrease at 9.5 (< pK_a = 9.65). Under such circumstances, the neutral form predominates, which is much more insoluble than its anionic counterpart present at pH 11.0. This was confirmed through an analogous EC trial upon pH regulated to 11.0. After 60 min, 27.1% BP-3 decay and 2.95% TOC reduction were found, values much lower than those obtained without pH regulation.

The effect of *j* on the performance of EC with Al/Al and Fe/Fe cells was further examined. It is expected that increasing *j* produces greater amounts of coagulants by acceleration of

electrode reactions (1)-(3), enhancing the removal of BP-3 and its products. Fig. 2a-d reveals BP-3 removals of 67.6%-71.4% and 57.0%-60.1% using Al/Al and Fe/Fe cells at 15 and 20 mA cm^{-2}. TOC abatements reached 54.1% for Al/Al cell at 15 mA cm^{-2} and 44.3% for the Fe/Fe one at 20 mA cm^{-2}, slightly > 41.3% found for 15 mA cm^{-2}. The fact that the Al/Al cell worked better at 15 mA cm^{-2} may be due to smaller BP-3 precipitation by the concomitant pH drop. The BP-3 removal was always larger than TOC abatement, meaning that BP-3 is rather transformed into byproducts by oxidation and reduction reactions, which are not so easily coagulated by $Al(OH)_3$ and $Fe(OH)_n$ flocs and become accumulated in the bulk.

To better clarify the superiority of the Al/Al cell to remove BP-3 at pH 11.0, the influence of the pollutant content was studied at 10-30 mg C L^{-1} at the optimum 15 mA cm^{-2}. Fig. S1a illustrates similar maximum BP-3 removal of 53.2%-58.3% starting at 10 and 20 mg C L^{-1}, raising substantially to 67.6% at 30 mg C L^{-1}. This agrees with the aforementioned precipitation of this molecule due to pH drop, occurring to larger extent at greater initial concentration. Similarly, Fig. S1b depicts a progressive increase of TOC decay from 39.7% to 54.1%, being again lower than BP-3 removal due to the formation of stable reduced and oxidized products.

Comparative EC trials using Na_2SO_4 were made to confirm the above behavior. With Fe/Fe cell, Fig. S2a and b reveals much larger BP-3 and TOC removals in simulated matrix as compared to EC in Na_2SO_4, since 57.0% and 39.4% were attained in the former medium, much larger than 41.3% and 20.1% in the latter one, which can be ascribed to additional oxidation with ClO^-. In Na_2SO_4, BP-3 also disappeared more quickly than TOC, as result of the simultaneous cathodic reduction and even by $^{\bullet}OH$-mediated oxidation of BP-3 (Thiam et al., 2014; Bocos et al., 2016). A smaller effect of the matrix was observed using Al/Al cell, where ca. 67 % BP-3 was removed from both media due to its precipitation upon pH drop, whereas TOC was abated more largely in the simulated matrix (54.1% vs. 44.6%), indicating the coagulation of products oxidized by ClO^-.

3.2. EC treatment of BP-3 in urban wastewater

The EC treatment of BP-3 was extended to an urban wastewater matrix at natural pH 8.0 (Table S1) using the Fe/Fe cell, envisaging its further combination with EAOPs. These tests were made with 4 mg C L^{-1} BP-3 (saturated solution of the neutral form) at 15 mA cm^{-2}.

Fig. 3a shows a dramatic BP-3 decay of 69.6% during the first 5 min of EC process, which was followed by an increase of BP-3 concentration so that only 40% was effectively removed from 20 min of electrolysis. In the first stage, the formation of complexes of the neutral form of BP-3 with some components of urban wastewater stimulate the rapid coagulation with $Fe(OH)_n$. The subsequent unexpected behavior arises from the gradual degradation of such natural components, causing the release of BP-3 entrapped in $Fe(OH)_n$ flocs to the bulk. The same trend was found using several pairs of Fe electrodes in parallel at 15 mA cm^{-2} each (data not shown), reinforcing the idea of BP-3 complexation. Conversely, this effect was not observed with Al/Al cell. Fig. S3 shows continuous BP-3 reduction by 50% in simulated matrix and urban wastewater at 15 mA cm^{-2}, similarly to that obtained with Fe/Fe cell (Fig. 3a). This indicates that the suggested complexes of BP-3 do not coagulate on $Al(OH)_3$ flocs.

Fig. 3b depicts gradual TOC abatement with the Fe/Fe cell, reaching 46.5% at 60 min, although 35% was attained at 15 min. To assess the decontamination, 6 cyclic compounds as soluble organic components after 20 min of electrolysis were identified by GC-MS (Table S4). All the molecules present in the raw wastewater (Table S2), except 2,2,6,6-tetramethyl-4-piperidinone and BP-3, were completely removed by EC. New molecules like dioxybenzone and 2-hydroxy-4-methoxybenzaldehyde appeared in the electrolyzed solution, coming from hydroxylation and cleavage of BP-3. This confirms the proposed concomitant production of $^{\bullet}OH$ during EC.

3.3. Degradation of BP-3 in urban wastewater by EAOPs

First, the ability of the air-diffusion cathode to electrogenerate H_2O_2 from reaction (7) (Brillas et al., 2009; Sirés et al., 2014) by the different EAOPs in the atypical media employed was investigated using a BDD anode and electrolyzing 100 mL samples of pH 8.0 at 33.3 mA cm^{-2} for 360 min.

$$O_2(g) + 2H^+ + 2e^- \rightarrow H_2O_2 \quad (7)$$

Fig. S4 highlights a gradual H_2O_2 accumulation over time in all cases. In EO-H_2O_2, 41.1 and 36.1 mM were finally obtained in the simulated matrix and urban wastewater. Oxidation of water at BDD anode originated physisorbed BDD($^\bullet$OH) by reaction (8) (Marselli et al., 2003; Özcan et al., 2008; Panizza and Cerisola, 2009), which reacted with H_2O_2 to form the weaker oxidant hydroperoxyl radical ($HO_2^\bullet$) via reaction (9) (Brillas et al., 2009; Sirés et al., 2014; Moreira et al., 2017). This caused its partial destruction, impeding higher accumulation. The smaller content obtained in urban wastewater suggests a slow H_2O_2 disappearance from reaction with some organic pollutants. When 10 mg L^{-1} Fe^{2+} was added to the urban wastewater (EF conditions), H_2O_2 was slowly accumulated up to 32.8 mM due to its additional removal from Fenton's reaction (10) (Dirany et al., 2011; El-Ghenymy et al., 2013; Olvera-Vargas et al., 2015). This content decreased to 24.9 mM under UVA irradiation in PEF mainly since Fenton's reaction (10) accelerated by Fe^{2+} regeneration from photolysis of soluble Fe(III) species by reaction (11) (Flox et al., 2007; Thiam et al., 2015; Zhang et al., 2016). These findings corroborate that sufficient H_2O_2 was produced in complex matrices for a large $^\bullet$OH generation in EAOPs.

$$BDD + H_2O \rightarrow BDD(^\bullet OH) + H^+ + e^- \quad (8)$$

$$BDD(^\bullet OH) + H_2O_2 \rightarrow BDD(HO_2^\bullet) + H_2O \quad (9)$$

$$Fe^{2+} + H_2O_2 \rightarrow Fe^{3+} + {}^\bullet OH + OH^- \quad (10)$$

$$Fe(OH)^{2+} + h\nu \rightarrow Fe^{2+} + {}^\bullet OH \quad (11)$$

The degradation of 4 mg C L^{-1} BP-3 in urban wastewater at natural pH 8.0 by EAOPs was performed under the above conditions. Fig 4a depicts the concentration decay using active RuO_2-based and non-active BDD anodes, as well as BP-3 was not photoactive upon UVA irradiation. At 33.3 mA cm^{-2}, this pollutant was more rapidly removed with BDD and, regardless of the anode, the oxidation ability rose as EO-H_2O_2 < EF < PEF, always disappearing in 45 min. These results indicate that in EO-H_2O_2, BP-3 was simultaneously degraded by ClO^- generated from Cl^- oxidation at each anode and by RuO_2(•OH) or, to a larger extent, by BDD(•OH). This agrees with the higher oxidation power expected for BDD (Brillas et al., 2009; Panizza and Cerisola, 2009; Sirés et al., 2014). The greater concentration decay in EF can be accounted for additional oxidation with •OH originated from Fenton's reaction (10), whereas the superiority of PEF is due to the larger production of •OH induced from reaction (11). However, good pseudo-first-order BP-3 kinetics were obtained in the case of EO-H_2O_2 (inset of Fig. 4a), with apparent rate constants of 0.075 min^{-1} (R^2 = 0.989) for RuO_2-based and 0.085 min^{-1} (R^2 = 0.995) for BDD. This behavior suggests a constant production of all oxidants, whereas the presence of Fe^{2+} in EF and PEF did not allow a clear kinetic analysis.

The action of oxidizing agents in each process was more evident from TOC profiles. Fig. 4b illustrates that BDD(•OH) always yielded much larger mineralization than RuO_2(•OH), then being BDD a better anode. The best mineralization with 62.6% TOC decrease was achieved by PEF, followed by 55.5% TOC removal by EF. The superiority of PEF is mainly due to the photolysis of some intermediates, including Fe(III) complexes of final carboxylic acids (Ruiz et al., 2011; Olvera-Vargas et al., 2015; Thiam et al., 2015). However, these products could only be confirmed in the case of EO-H_2O_2, where maleic and oxalic acids were identified by ion-exclusion HPLC. Fig. 5a and b shows the time course of these acids using RuO_2-based and BDD anodes. Their low content (< 0.50 mg C L^{-1}) suggests that all treated solutions contained

297 a mixture of recalcitrant molecules coming from the degradation of BP-3 and organic
298 components of wastewater.

299 Fe^{2+} concentration and pH are two key parameters in Fenton-based EAOPs since they
300 modulate •OH production from Fenton's reaction (10) (Brillas et al., 2009; Sirés et al., 2014;
301 Martínez-Huitle et al., 2015). Fig. 6a and b show a little effect of Fe^{2+} content on BP-3
302 degradation at natural pH in EF and PEF operating from 10 to 28 mg L^{-1}. A slightly better
303 performance was achieved with 10 mg L^{-1} Fe^{2+}, suggesting lower •OH production at the highest
304 Fe^{2+} content due to precipitation of the excess of iron ions at such high pH, which caused partial
305 destruction of H_2O_2 by heterogeneous reaction (Brillas et al., 2009). Conversely, Fig. 6c and d
306 reveal quicker degradation at pH 3.0 (optimum pH for Fenton's reaction (10)) (Brillas et al.,
307 2009), for both treatments with 28 mg L^{-1} Fe^{2+}. BP-3 disappeared in 20 min, a time < 45 min at
308 pH 8.0 (Fig. 6a), and TOC was more largely reduced by 64.4% in EF and 72.5% in PEF. The
309 superiority of BP-3 degradation at optimum pH 3.0 as compared to pH 8.0 is due to the faster
310 degradation in the presence of larger amounts of •OH produced, either with BP-3, the organic
311 components of urban wastewater or their products. Moreover, HClO was the dominant active
312 chlorine species at pH 3.0, with much higher oxidation power than ClO^- formed at pH 8.0 (Sirés
313 et al., 2014).

314 *3.4. Detection of primary intermediates upon BP-3 degradation in a simulated water matrix*

315 The primary intermediates generated from BP-3 (**1**) were identified in simulated water by
316 GC-MS analysis of organic components produced after 2 min of PEF of 4 mg C L^{-1} BP-3 at pH
317 8.0 using BDD/air-diffusion cell at 33.3 mA cm^{-2}. Table S5 summarizes 14 cyclic molecules
318 detected, including two direct hydroxylated derivatives of the parent molecule (**2** and **3**), three
319 xanthene derivatives, non-chlorinated (**4**) or chloroderivatives (**6** and **7**), one dibenzenic
320 intermediate (**14**), four monobenzenic intermediates (**5**, **11**, **12** and **13**) and four chlorobenzenic

derivatives (**8**, **9**, **10** and **15**). Note that **2** and **5** were also formed during EC treatment of BP-3 (Table S4). The mass spectra of these products are given in Fig. S5.

From the above byproducts, a reaction sequence for the initial BP-3 degradation is proposed in Fig. 7. It can be valid for all EAOPs tested, since their main oxidants are hydroxyl radicals (BDD(•OH) and •OH), represented as •OH for the sake of simplicity, and active chlorine ($HClO/ClO^-$). The route is initiated by hydroxylation of **1** either at position C-2' to yield **2** or at position C-4 to give **3** with loss of methoxy group. Further hydroxylation of **2** causes cyclization to form the xanthenone **4** or cleavage of the C(1')-CO bond to produce the benzaldehyde **5**. Chlorination of **4** yields consecutively the xanthenes derivatives **6** and **7**, which undergo hydroxylation with cleavage of the cyclic structure to yield the benzenic compound **8**. This byproduct is subsequently chlorinated to **9**, finally transformed into **10** via hydroxylation/chlorination with release of Cl^- and methoxy groups. On the other hand, hydroxylation of the aromatic rings of **3** causes its cleavage to yield **11** and **12**, whereas the attack of •OH onto the CO group of **3** promotes acid **13**. An esterification of **13** with an intermediate of **8** (possibly, 4-chlorophenol, resulting from the loss of methoxy group), yielded **14**. Alternatively, **13** may be converted into the chlorinated compound **15**.

3.5. Sequential EC/EF and EC/PEF treatments of BP-3 in urban wastewater

From the results for EC, j = 15 mA cm^{-2} and 20 min of electrolysis were chosen to electrolyze 150 mL of 4 mg C L^{-1} BP-3 spiked into urban wastewater at natural pH 8.0 using the Fe/Fe cell before treatment by EF and PEF. Fig. 8a and b depicts that 41% of BP-3 and 36% of TOC were removed by this pre-treatment, with total soluble iron of 7 mg L^{-1} and final pH 8.2. EAOPs were then performed with 100 mL of supernatant liquid using BDD/air-diffusion cell at 33.3 mA cm^{-2} for 360 min. Fig. 8a shows that BP-3 disappeared after 45 min of EF and PEF, as well as in PEF with 10 mg L^{-1} Fe^{2+}, all at natural pH. These results agree with the behavior of both single processes, meaning that BDD(•OH), ClO^- and •OH in the bulk are the

main oxidants, without significant influence of Fe^{2+} addition since the catalyst supplied by EC is enough for an effective Fenton's reaction (10) to produce •OH at this pH. Fig. 8a also shows a notable influence of pH on BP-3 removal, disappearing at 10 min by PEF with 10 mg L^{-1} Fe^{2+} at pH 3.0 due to the greater production of •OH by enhancement of Fenton's reaction (10) and simultaneous oxidation by HClO. In the same assays, Fig. 8b illustrates final TOC abatements of 72.5% by EF, about 80% in both PEF at natural pH, and 87.3% in PEF at pH 3.0. The larger mineralization by PEF can be associated with the photolysis of some products upon UVA irradiation that enhances its transformation into CO_2, whereas the superiority of PEF at pH 3.0 can be related again to the larger •OH generation and the presence of HClO.

To confirm the benefits of sequential EC/PEF, additional experiments to reach total mineralization (> 99% TOC reduction) were made. Fig. 9 reveals that urban wastewater was totally decontaminated in 820 min by PEF at natural pH by adding 10 mg L^{-1} Fe^{2+}. Shorter times of 720 and 680 min were required using EC/PEF, with PEF performed at natural pH or at pH 3.0. As expected, faster mineralization was achieved at pH 3.0 owing to the reasons exposed above. Sequential EC/PEF at natural pH is then more useful in practice than single PEF because lower electrical consumption is needed to mineralize all contaminants. On the other hand, the final sludge of the EC pre-treatment should be managed conveniently.

For the most powerful sequential EC/PEF treatment at natural pH, the average cell voltages (E_{cell}) listed in Table S3 allowed determining the energy consumption, as explained elsewhere (Thiam et al., 2015). A low value of 2.36 kWh m^{-3} resulted in the EC pre-treatment, in contrast to much greater values of 172.8 and 345.6 kWh m^{-3} for the subsequent PEF treatment at 360 and 720 min. These high consumptions could be reduced down to 136.8 and 273.6 kWh m^{-3} upon replacement of the UVA lamp by sunlight, as proposed in earlier papers (Flox et al., 2007; Salazar et al., 2012; Brillas, 2014).

4. Conclusions

- The Al/Al cell was proven as optimal for EC treatment of BP-3 in simulated matrix at pH 11.0 due to: (i) precipitation of the neutral form of BP-3 from pH decrease, (ii) coagulation of the anionic form with hydroxide flocs, (iii) reductive transformation and (iv) oxidation of BP-3 and its byproducts by generated ClO^- and $^{\bullet}OH$. The three latter processes occurred in the Fe/Fe cell as well.
- BP-3 spiked into urban wastewater at natural pH 8.0 treated by EC with Fe/Fe cell at 15 mA cm^{-2} showed a dramatic content decay thanks to coagulation of its complexes with components of the wastewater, followed by partial BP-3 redissolution when they were oxidized by $^{\bullet}OH$ and ClO^-.
- The oxidation power of EAOPs in this real sample rose as EO-H_2O_2 < EF < PEF, with larger effectiveness of the BDD/air-diffusion cell than using a RuO_2-based anode. The superiority of PEF was due to additional photolysis of intermediates.
- The organic molecules identified upon EC and EAOPs revealed a certain oxidation ability of EC process.
- The sequential EC (Fe/Fe cell, 15 mA cm^{-2}, 20 min)/PEF (BDD/air-diffusion cell, 33.3 mA cm^{-2}, 360 min) of BP-3-loaded urban wastewater at natural pH was much more powerful than EC/EF. The time needed for total mineralization by EC/PEF was shorter than in single PEF, then being sequential electrochemical processes a very interesting alternative.

Acknowledgements

The authors thank financial support from project CTQ2016-78616-R (AEI/FEDER, EU) and PhD scholarship awarded to Z. Ye (State Scholarship Fund, CSC, China). J.R. Steter thanks funding from process number 234142/2014-6 (CNPq, Brazil).

394 **References**

395 Abdallah, P., Deborde, M., Berne, F.D., Leitner, N.K.V., 2015. Kinetics of chlorination of
396 benzophenone-3 in the presence of bromide and ammonia. Environ. Sci. Technol. 49
397 (24), 14359-14367.

398 Asghar, A., Raman, A.A.A., Daud, W.M.A.W., 2015. Advanced oxidation processes for in-situ
399 production of hydrogen peroxide/hydroxyl radical for textile wastewater treatment: a
400 review. J. Clean. Prod. 87, 826-838.

401 Bocos, E., Brillas, E., Sanromán, M.A., Sirés, I., 2016. Electrocoagulation: Simply a phase
402 separation technology? The case of bronopol compared to its treatment by
403 EAOPs. Environ. Sci. Technol. 50 (14), 7679-7686.

404 Brillas, E., 2014. A review on the degradation of organic pollutants in waters by UV
405 photoelectro-Fenton and solar photoelectro-Fenton. J. Braz. Chem. Soc. 25 (3), 393-417.

406 Brillas, E., Martínez-Huitle, C.A., 2015. Decontamination of wastewaters containing synthetic
407 organic dyes by electrochemical methods. An updated review. Appl. Catal. B: Environ.
408 166-167, 603-643.

409 Brillas, E., Sirés, I., Oturan, M.A., 2009. Electro-Fenton process and related electrochemical
410 technologies based on Fenton's reaction chemistry. Chem. Rev. 109 (12), 6570-6631.

411 Cheng, M., Lai, C., Liu, Y. Zeng, G., Huang, D., Zhang, C., Qin, L., Hu, L., Zhou, C., Xiong,
412 W., 2018a. Metal-organic frameworks for highly efficient heterogeneous Fenton-like
413 catalysis. Coord. Chem. Rev. 368, 80-92.

414 Cheng, M., Zeng, G., Huang, D., Lai, C., Liu, Y., Zhang, C., Wan, J., Hu, L., Zhou, C., Xiong,
415 W., 2018b. Efficient degradation of sulfamethazine in simulated and real wastewater at
416 slightly basic pH values using Co-SAM-SCS /H_2O_2 Fenton-like system. Water Res. 138,
417 7-18.

418 Cheng, M., Zeng, G., Huang, D., Lai, C., Xu, P., Zhang, C., Liu, Y., Wan, J., Gong, X., Zhu,
419 Y., 2016. Degradation of atrazine by a novel Fenton-like process and assessment the
420 influence on the treated soil. J. Hazard. Mater. 312, 184-191.
421 Demirbas, E., Kobya, M., 2017. Operating cost and treatment of metalworking fluid wastewater
422 by chemical coagulation and electrocoagulation processes. Process Saf. Environ. Prot.
423 105, 79-90.
424 Dirany, A., Efremova Aaron, S., Oturan, N., Sirés, I., Oturan, M.A., Aaron, J.J., 2011. Study of
425 the toxicity of sulfamethoxazole and its degradation products in water by a
426 bioluminescence method during application of the electro-Fenton treatment. Anal.
427 Bioanal. Chem. 400 (2), 353-360.
428 Downs, C.A., Kramarsky-Winter, E., Segal, R., Fauth, J., Knutson, S., Bronstein, O., Ciner,
429 F.R., Jeger, R., Lichtenfeld, Y., Woodley, C.M., Pennington, P., Cadenas, K., Kushmaro,
430 A., Loya, Y., 2016. Toxicopathological effects of the sunscreen UV filter, oxybenzone
431 (benzophenone-3), on coral planulae and cultured primary cells and its environmental
432 contamination in Hawaii and the U.S. Virgin Islands, Arch. Environ. Contam. Toxicol.
433 70 (2), 265-288.
434 El-Ashtoukhy, E.-S.Z., Amin, N.K., Abd El-Latif, M.M., Bassyouni, D.G., Hamad, H.A., 2017.
435 New insights into the anodic oxidation and electrocoagulation using a self-gas stirred
436 reactor: A comparative study for synthetic C.I Reactive Violet 2 wastewater. J. Clean.
437 Prod. 167, 432-446.
438 El-Ghenymy, A., Oturan, N., Oturan, M.A., Garrido, J.A., Cabot, P.L., Centellas, F., Rodríguez,
439 R.M., Brillas, E., 2013. Comparative electro-Fenton and UVA photoelectro-Fenton
440 degradation of the antibiotic sulfanilamide using a stirred BDD/air-diffusion tank reactor.
441 Chem. Eng. J. 234, 115-123.

Flox, C., Garrido, J.A., Rodríguez, R.M., Cabot, P.L., Centellas, F., Arias, C., Brillas, E., 2007. Mineralization of herbicide mecoprop by photoelectro-Fenton with UVA and solar light. Catal. Today 129 (1-2), 29-36.

Gago-Ferrero, P., Demeestere, K., Díaz-Cruz, M.S., Barceló, D., 2013. Ozonation and peroxone oxidation of benzophenone-3 in water: Effect of operational parameters and identification of intermediate products. Sci. Total Environ. 443, 209-217.

Ghernaout, D., 2013. Advanced oxidation phenomena in electrocoagulation process: a myth or a urbanity?. Desalination Water Treat. 51 (40-42), 7536-7554.

Ghernaout, D., Naceur, M.W., Aouabed, A., 2011. On the dependence of chlorine by-products generated species formation of the electrode material and applied charge during electrochemical water treatment. Desalination 270 (1-3), 9-22.

Gilberta, E., Roussela, L., Serre, C., Sandouk, R., Salmon, D., Kirilov, P., Haftek, M., Falson, F. Pirot, F., 2016. Percutaneous absorption of benzophenone-3 loaded lipid nanoparticles and polymeric nanocapsules: A comparative study. Int. J. Pharm. 504 (1-2), 48-58.

Gong, P., Yuan, H., Zhai, P., Xue, Y., Li, H., Dong, W., Mailhot, G., 2015. Investigation on the degradation of benzophenone-3 by UV/H_2O_2 in aqueous solution. Chem. Eng. J. 277, 97-103.

Guo, Y., Xu, B., Qi, F., 2016. A novel ceramic membrane coated with MnO_2–Co_3O_4 nanoparticles catalytic ozonation for benzophenone-3 degradation in aqueous solution: Fabrication, characterization and performance. Chem. Eng. J. 287, 381-389.

Khandegar, V., Saroha, A.K., 2013. Electrocoagulation for the treatment of textile industry effluent--a review. J. Environ. Manage. 128, 949-963.

Li, Y.J., Qiao, X.L., Zhou, C.Z., Zhang, Y.N., Fu, Z.Q., Chen, J.W., 2016. Photochemical transformation of sunscreen agent benzophenone-3 and its metabolite in surface freshwater and seawater. Chemosphere 153, 494-499.

Liu, Y.S., Ying, G.G., Shareef, A., Kookana, R.S., 2012. Biodegradation of the ultraviolet filter benzophenone-3 under different redox conditions. Environ. Toxicol. Chem. 31 (2), 289-295.

Marselli, B., Garcia-Gomez, J., Michaud, P.A., Rodrigo, M.A., Comninellis, C., 2003. Electrogeneration of hydroxyl radicals on boron-doped diamond electrodes. J. Electrochem. Soc. 150 (3), D79-D83.

Martínez-Huitle, C.A., Rodrigo, M.A., Sirés, I., Scialdone, O., 2015. Single and coupled electrochemical processes and reactors for the abatement of organic water pollutants: A critical review. Chem. Rev. 115 (24), 13362–13407.

Moreira, F.C., Boaventura, R.A.R, Brillas, E., Vilar, V.J.P., 2017. Electrochemical advanced oxidation processes: A review on their application to synthetic and urban wastewaters. Appl. Catal. B: Environ. 202, 217-261.

Olvera-Vargas, H., Oturan, N., Oturan, M.A., Brillas, E., 2015. Electro-Fenton and solar photoelectro-Fenton treatments of the pharmaceutical ranitidine in pre-pilot flow plant scale. Separ. Purif. Technol. 146, 127-135.

Özcan, A., Şahin, Y., Koparal, A.S., Oturan, M.A., 2008. Propham mineralization in aqueous medium by anodic oxidation using boron-doped diamond anode. Experimental parameters' influence on degradation kinetics and mineralization efficiency. Water Res. 42 (12), 2889-2898.

Panizza, M., Cerisola, G., 2009. Direct and mediated anodic oxidation of organic pollutants. Chem. Rev. 109 (12), 6541-6569.

Ridruejo, C., Salazar, C., Cabot, P.L., Centellas, F., Brillas, E., Sirés, I., 2017. Electrochemical oxidation of anesthetic tetracaine in aqueous medium. Influence of the anode and matrix composition. Chem. Eng. J. 326, 811-819.

Ruiz, E.J., Hernández-Ramírez, A., Peralta-Hernández, J.M., Arias, C., Brillas, E., 2011. Application of solar photoelectro-Fenton technology to azo dyes mineralization: Effect of current density, Fe^{2+} and dye concentration. Chem. Eng. J. 171 (2), 385-392.

Salazar, R., Brillas, E., Sirés, I., 2012. Finding the best Fe^{2+}/Cu^{2+} combination for the solar photoelectro-Fenton treatment of simulated wastewater containing the industrial textile dye Disperse Blue 3. Appl. Catal. B: Environ. 115–116, 107-116.

Särkkä, H., Bhatnagar, A., Sillanpää, M., 2015. Recent developments of electro-oxidation in water treatment - A review. J. Electroanal. Chem. 754, 46-56.

Silva, L.G.M., Moreira, F.C., Souza, A.A.U., Souza, S.M.A.G.U., Boaventura, R.A.R., Vilar, V.J.P., 2018. Chemical and electrochemical advanced oxidation processes as a polishing step for textile wastewater treatment: A study regarding the discharge into the environment and the reuse in the textile industry. J. Clean. Prod. 198, 430-442.

Sirés, I., Brillas, E., Oturan, M.A., Rodrigo, M.A., Panizza, M., 2014. Electrochemical advanced oxidation processes: Today and tomorrow. Environ. Sci. Pollut. Res. 21 (14), 8336-8367.

Steter, J.R., Brillas, E., Sirés, I., 2016. On the selection of the anode material for the electrochemical removal of methylparaben from different aqueous media. Electrochim. Acta 222, 1464-1474.

Thiam, A., Sirés, I., Brillas, E., 2015. Treatment of a mixture of food color additives (E122, E124 and E129) in different water matrices by UVA and solar photoelectro-Fenton. Water Res. 81, 178-187.

Thiam, A., Zhou, M., Brillas, E., Sirés, I., 2014. Two-step mineralization of Tartrazine solutions: Study of parameters and by-products during the coupling of electrocoagulation with electrochemical advanced oxidation processes. Appl. Catal. B: Environ. 150-151, 116-125.

516 Urzúa, J., González-Vargas, C., Sepúlveda, F., Ureta-Zañartu, M.S., Salazar, R., 2013.
517 Degradation of conazole fungicides in water by electrochemical oxidation. Chemosphere
518 93 (11), 2774-2781.
519 Wang, A., Qu, J., Liu, H., Ru, J., 2008. Mineralization of an azo dye Acid Red 14 by
520 photoelectro-Fenton process using an activated carbon fiber cathode. Appl. Catal. B:
521 Environ. 84 (3-4), 393-399.
522 Welcher, F.J. (Ed.), 1975. Standard Methods of Chemical Analysis, Part B, vol. 2, sixth ed.,
523 R.E. Krieger Pub. Co., New York, p. 1827.
524 Zhang, Y., Wang, A., Tian, X., Wen, Z., Lv, H., Li, D., Li, J., 2016. Efficient mineralization of
525 the antibiotic timethoprim by solar assisted photoelectro-Fenton process driven by a
526 photovoltaic cell. J. Hazard. Mater. 318, 319-328.
527 Zúñiga-Benítez, H., Aristizábal-Ciro, C., Peñuela, G.A., 2016a. Heterogeneous photocatalytic
528 degradation of the endocrine-disrupting chemical benzophenone-3: Parameters
529 optimization and by-products identification. J. Environ. Manage. 167, 246-258.
530 Zúñiga-Benítez, H., Aristizábal-Ciro, C., Peñuela, G.A., 2016b. Photodegradation of the
531 endocrine-disrupting chemicals benzophenone-3 and methylparaben using Fenton
532 reagent: Optimization of factors and mineralization/biodegradability studies. J. Taiwan
533 Inst. Chem. Eng. 59, 380-388.
534 Zúñiga-Benítez, H., Soltan, J., Peñuela, G.A., 2016c. Application of ultrasound for degradation
535 of benzophenone-3 in aqueous solutions. Int. J. Environ. Sci. Technol. 13 (1), 77-86.
536

Figure captions

Fig. 1. Normalized TOC decay for the EC treatment of 150 mL of 30 mg C L^{-1} BP-3 in simulated matrix at pH 11.0 and 35 ºC using anode/cathode cells (10 cm^2 electrode area) at 10 mA cm^{-2}. Anode: (a) Al and (b) Fe.

Fig. 2. Normalized (a,c) BP-3 concentration and (b,d) TOC abatements for the solution of Fig. 1 of pH 11.0, treated by EC with (a,b) Al/Al and (c,d) Fe/Fe cells. Current density: (●) 5 mA cm^{-2}, (■) 10 mA cm^{-2}, (▲) 15 mA cm^{-2} and (▼) 20 mA cm^{-2}.

Fig. 3. Normalized (a) BP-3 concentration and (b) TOC removals for the EC treatment of 150 mL of 4 mg C L^{-1} BP-3 in urban wastewater at natural pH 8.0 and 35 ºC using Fe/Fe cell at 15 mA cm^{-2}.

Fig. 4. Change of normalized (a) BP-3 concentration and (b) TOC for the treatment of 100 mL of 4 mg C L^{-1} BP-3 in urban wastewater at natural pH 8.0 and 35 ºC using (○,□,△) RuO_2-based/air-diffusion and (●,■,▲) BDD/air-diffusion cells at 33.3 mA cm^{-2}. Method: (○,●) EO-H_2O_2, (□,■) EF with 10 mg L^{-1} Fe^{2+} and (△,▲) PEF with 10 mg L^{-1} Fe^{2+} and 6 W UVA irradiation. (◆) Only 6 W UVA irradiation.

Fig. 5. Time course of (a) maleic and (b) oxalic acids concentration during the EO-H_2O_2 of the sample of Fig. 4 using (○) RuO_2-based/air-diffusion and (●) BDD/air-diffusion cells.

Fig. 6. Normalized (a,c) BP-3 concentration and (b,d) TOC decays for 100 mL of 4 mg C L^{-1} BP-3 in urban wastewater using BDD/air-diffusion cell at 33.3 mA cm^{-2} and 35 ºC. (a,b) Natural pH 8.0: EF with (○) 10 and (□) 28 mg L^{-1} Fe^{2+}, and PEF with (●) 10 and (■) 28 mg L^{-1} Fe^{2+}. (c,d) pH 3.0: (△) EF and (▲) PEF, both with 28 mg L^{-1} Fe^{2+}.

Fig. 7. Proposed reaction sequence for the initial degradation of BP-3 by EAOPs, tested in simulated water matrix.

Fig. 8. Normalized (a) BP-3 concentration and (b) TOC decays for sequential EC/EAOPs treatment of 4 mg C L^{-1} BP-3 in urban wastewater at 35 ºC. (◆) EC pre-treatment of 150 mL at natural pH 8.0 using Fe/Fe cell at 15 mA cm^{-2} for 20 min. Further degradation of 100 mL of supernatant liquid using BDD/air-diffusion cell at 33.3 mA cm^{-2} by: (○) EF and (□) PEF, both without addition of Fe^{2+}, (■) PEF with 10 mg L^{-1} Fe^{2+} and (▲) PEF at pH 3.0 with 10 mg L^{-1} Fe^{2+}.

Fig. 9. Normalized TOC removal for 4 mg C L^{-1} BP-3 in urban wastewater at 35 ºC. (▲) 100 mL at natural pH 8.0 with addition of 10 mg L^{-1} Fe^{2+}, treated by PEF with BDD/air-diffusion cell at 33.3 mA cm^{-2}. EC/PEF process: (◆) 150 mL of wastewater pre-treated by EC with Fe/Fe cell at 15 mA cm^{-2} for 20 min, followed by PEF treatment of 100 mL of supernatant liquid at (●) natural pH and (■) pH 3.0 with BDD/air-diffusion cell.

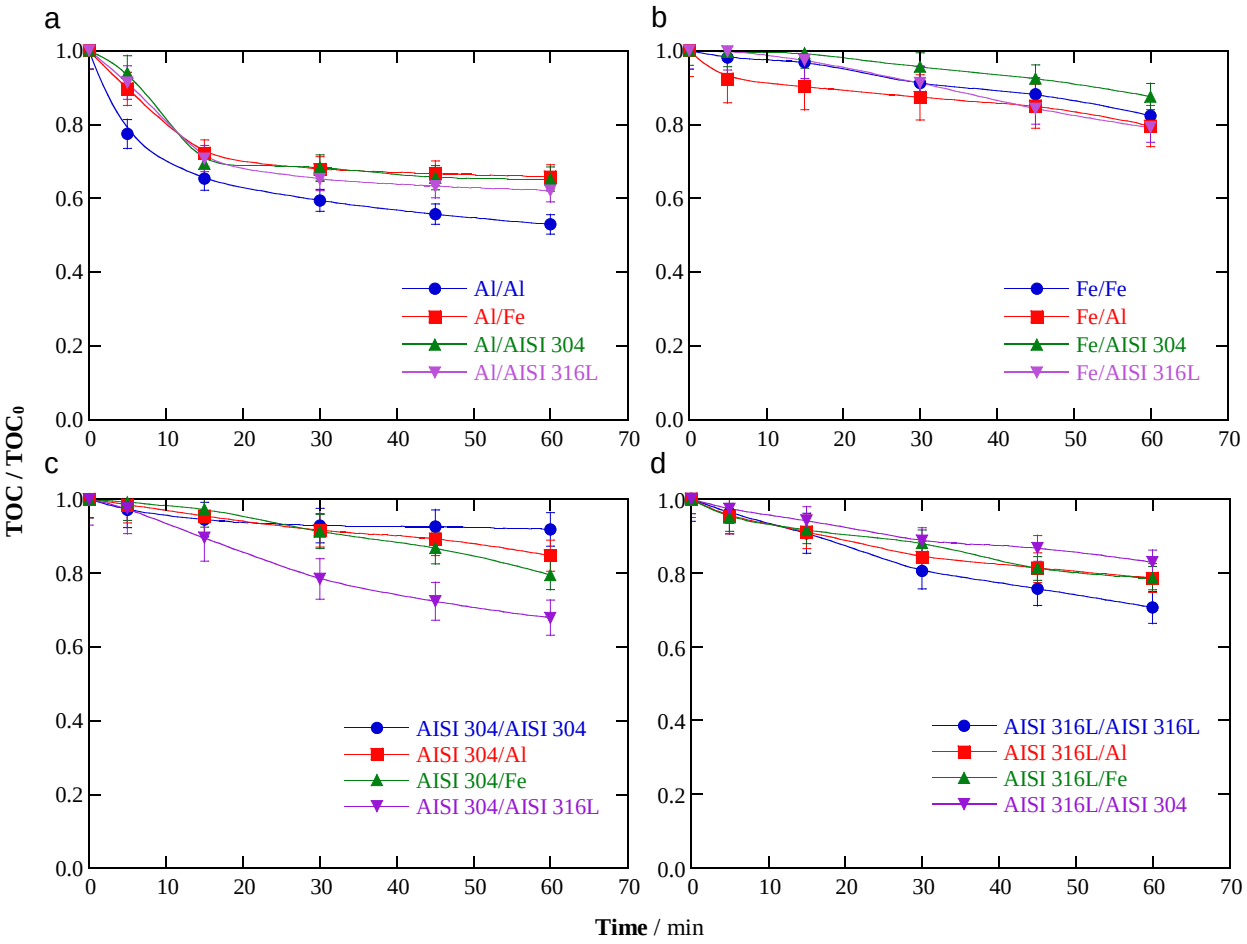
a
b
c
d
TOC / TOC0
Time / min
Al/Al
Al/Fe
Al/AISI 304
Al/AISI 316L
Fe/Fe
Fe/Al
Fe/AISI 304
Fe/AISI 316L
AISI 304/AISI 304
AISI 304/Al
AISI 304/Fe
AISI 304/AISI 316L
AISI 316L/AISI 316L
AISI 316L/Al
AISI 316L/Fe
AISI 316L/AISI 304

Fig. 1

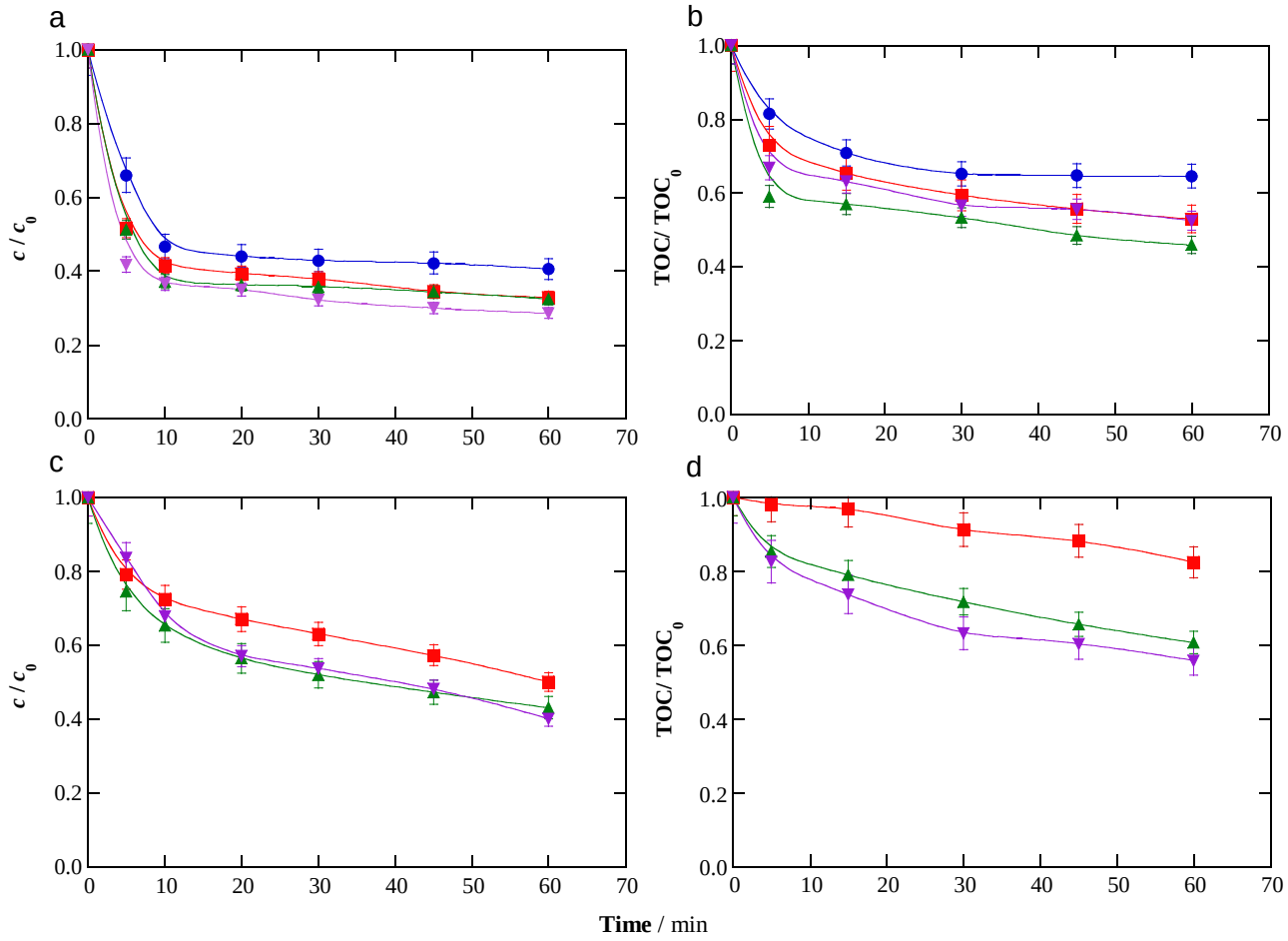

Fig. 2

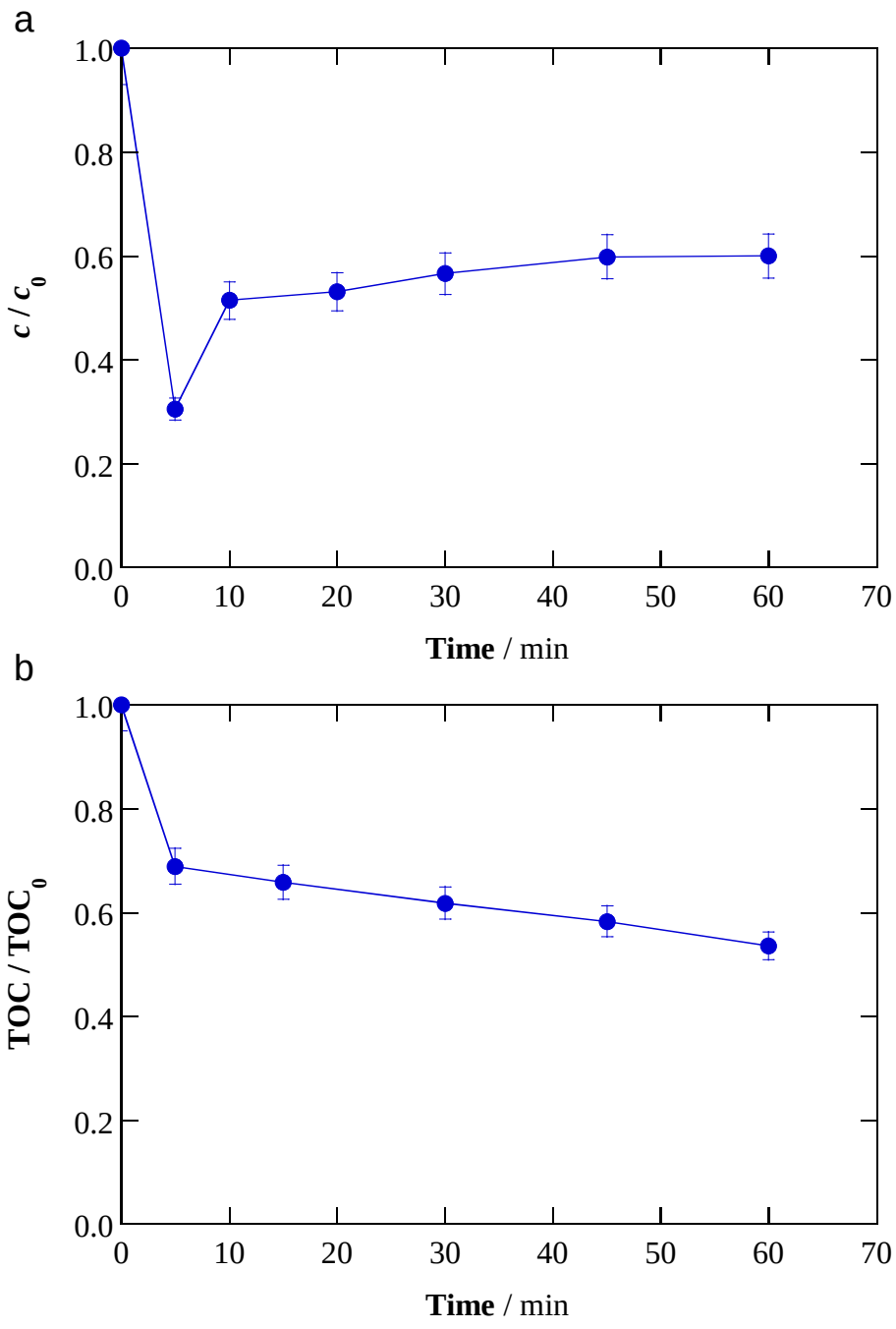
a
1.0
0.8
0.6
0.4
0.2
0.0
c / c0
0
10
20
30
40
50
60
70
Time / min
b
1.0
0.8
0.6
0.4
0.2
0.0
TOC / TOC0
0
10
20
30
40
50
60
70
Time / min

Fig. 3

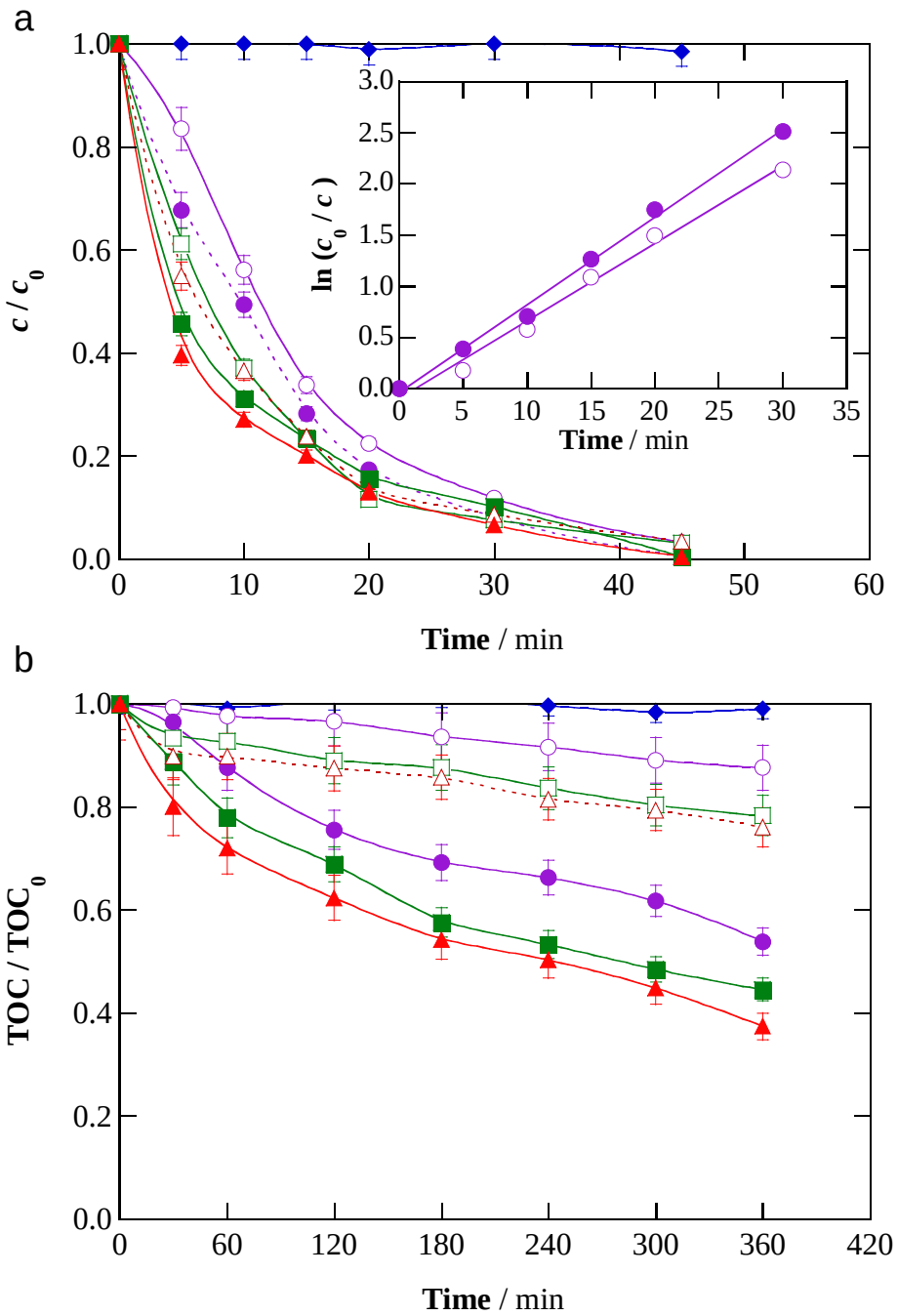
a
1.0
0.8
0.6
0.4
0.2
0.0
c / c0
0
10
20
30
40
50
60
Time / min
3.0
2.5
2.0
1.5
1.0
0.5
0.0
ln (c0 / c)
0
5
10
15
20
25
30
35
Time / min
b
1.0
0.8
0.6
0.4
0.2
0.0
TOC / TOC0
0
60
120
180
240
300
360
420
Time / min

Fig. 4

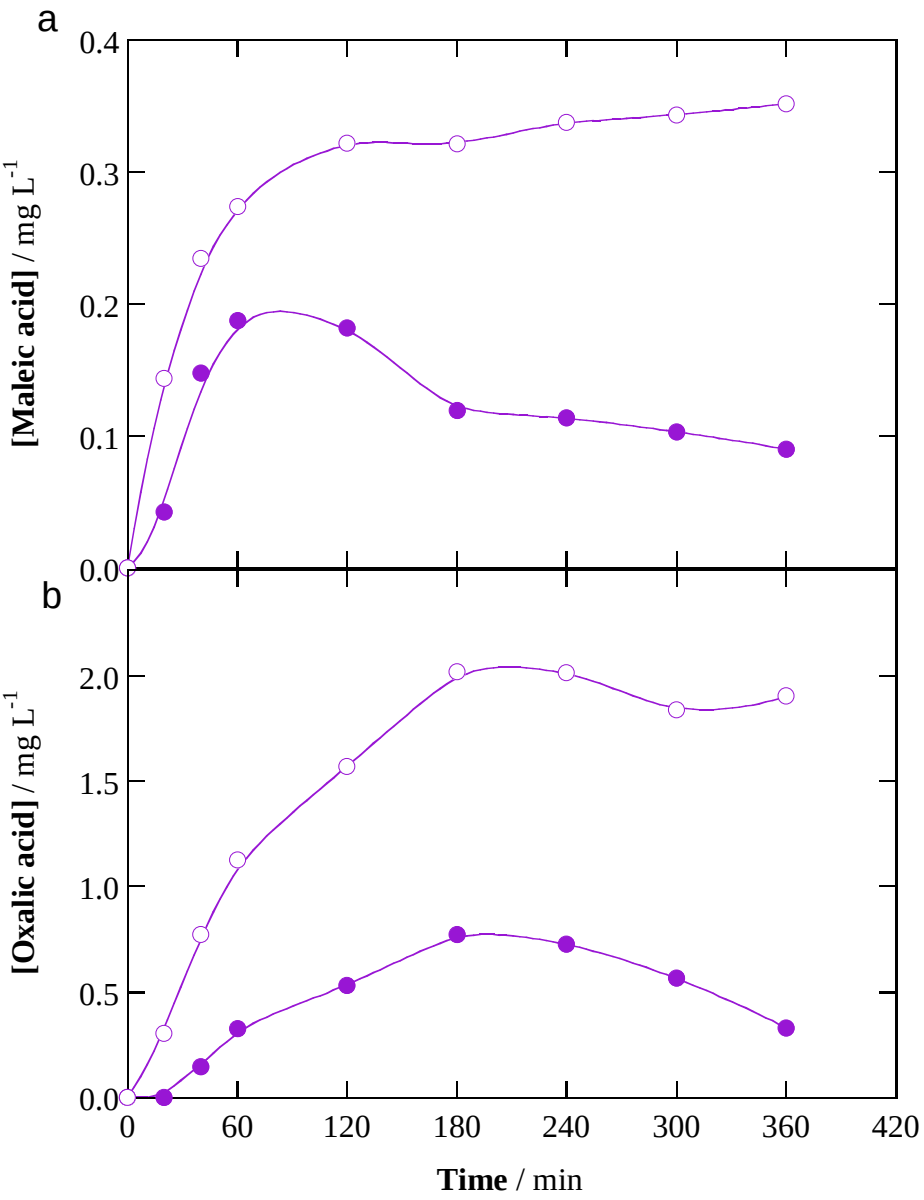
a
b
[Maleic acid] / mg L-1
[Oxalic acid] / mg L-1
0.0
0.1
0.2
0.3
0.4
0.5
1.0
1.5
2.0
0
60
120
180
240
300
360
420
Time / min

Fig. 5

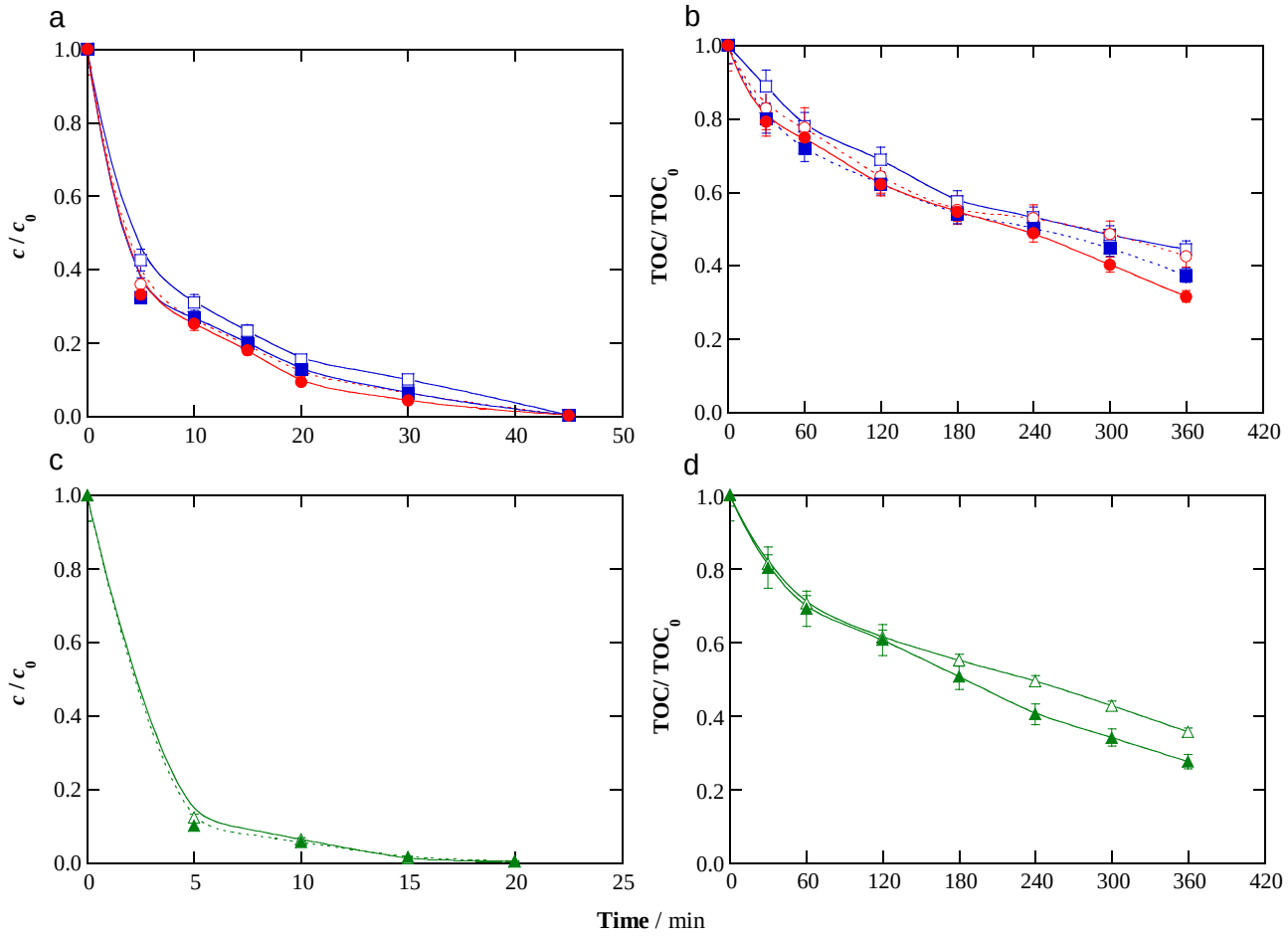

Fig. 6

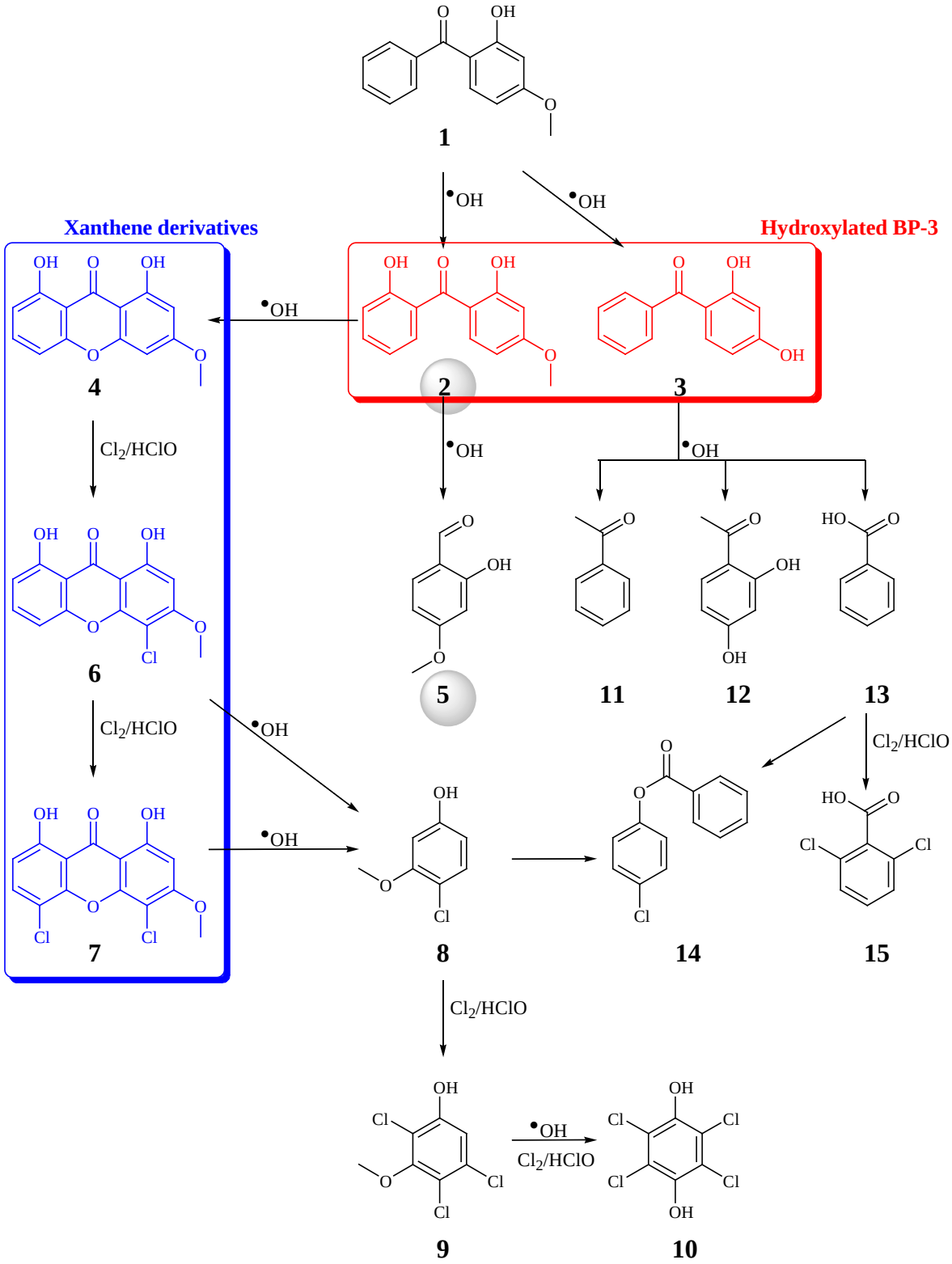
Xanthene derivatives
Hydroxylated BP-3
1
2
3
4
5
6
7
8
9
10
11
12
13
14
15
•OH
Cl2/HClO

Fig. 7

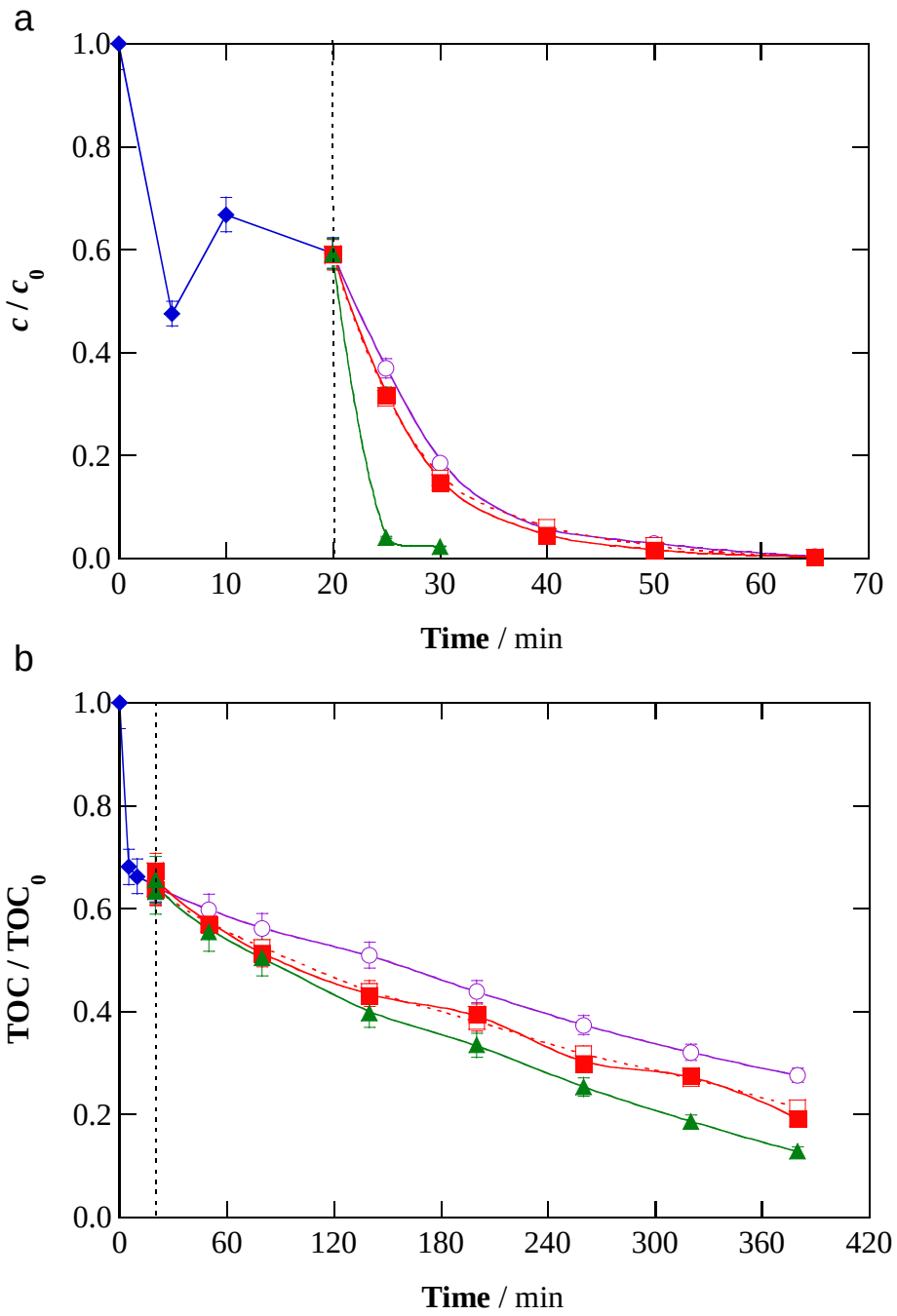
a
1.0
0.8
0.6
0.4
0.2
0.0
c / c0
0
10
20
30
40
50
60
70
Time / min
b
1.0
0.8
0.6
0.4
0.2
0.0
TOC / TOC0
0
60
120
180
240
300
360
420
Time / min

Fig. 8

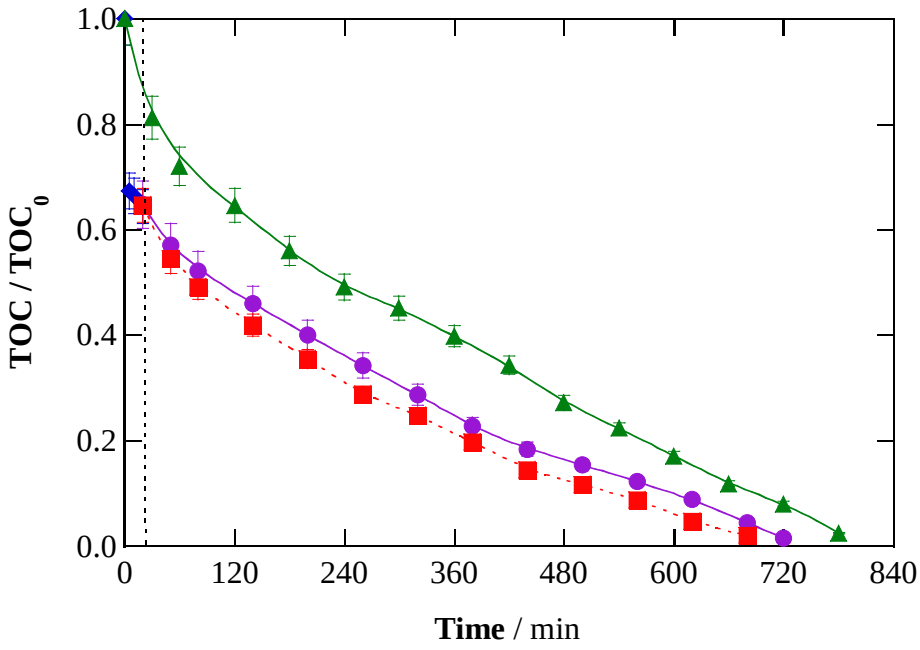

Fig. 9